Simultaneous suppression of superfluid and resistance on approach to superconductor-insulator transition in underdoped ultrathin Ca$_{0.3}$Y$_{0.7}$Ba$_2$Cu$_3$O$_{7-\delta}$ films

S. Steers,[*] T. R. Lemberger, and J. Draskovic

Department of Physics, The Ohio State University, 191 Woodruff Avenue, Columbus, Ohio 43210, USA

Using simple four-terminal resistance measurements and two-coil superfluid stiffness measurements, we observe an extended temperature range wherein both the superfluid density and the resistance are substantially suppressed, in some cases below experimental resolution, in severely underdoped ultrathin films of Ca$_{0.3}$Y$_{0.7}$Ba$_2$Cu$_3$O$_{7-\delta}$ (CaYBCO). This temperature range δT_c, deemed the "offset," is in some films more than $\frac{1}{2}$ of the resistive transition temperature. δT_c scales linearly with the characteristic two-dimensional (2D) vortex unbinding temperature T_{2D}, growing larger with underdoping upon approach to the superconductor-insulator transition. Absent in three-dimensional samples of CaYBCO, we discuss the offset in the context of a previously observed 2D quantum critical point in the vicinity of the superconductor-insulator transition, as well as in the context of intrinsic and extrinsic inhomogeneities in the superconducting state of the film.

I. INTRODUCTION

In the cuprate family of high-temperature superconductors, which fluctuations are primarily responsible for the collapse of the superconducting state has been a widely debated topic. For a particular hole doping, it is unclear whether thermal fluctuations drive both the amplitude and the phase of the order parameter to zero, or whether the phase alone is suppressed to zero, with some authors suggesting that the pairing amplitude is nonzero at temperatures far exceeding T_c. Further complicating the picture are quantum critical fluctuations arising from the approach to a quantum critical point (QCP), in this case a superconductor-insulator transition (SIT), with decreasing hole doping. These quantum critical fluctuations affect the number of electrons that enter the superconducting state [1,2], thereby decreasing the energy associated with changes in the phase of the order parameter. Dimensionality can add yet another layer of complication to the forms the various fluctuations may take, especially given the highly anisotropic layered structure of the cuprates. Thus, not only must multiple parameters (e.g., temperature, doping, thickness) be varied to disentangle the contributions of different fluctuations, but comparisons must be made between measurements sensitive to different aspects of the system. In this work, we focus on ultrathin films of Ca$_{0.3}$Y$_{0.7}$Ba$_2$Cu$_3$O$_{7-\delta}$ (CaYBCO), seeking to compare measurements of the superfluid density with the resistivity. Given previous work establishing the presence of two-dimensional (2D) phase fluctuations in the disappearance of the superfluid density [1], (specifically, vortex/antivortex pair production), comparison of the superfluid and resistivity data for these films could shed light on the prominence of 2D thermal phase fluctuations near the SIT.

Two-dimensional thermal fluctuations of the phase in the form of vortex singularities have been known since the theoretical work of Kosterlitz and Thouless and Berezinskii [3–5]. Tightly bound pairs of vortices and antivortices (having opposite magnetic moments and corresponding to the conservation of magnetic flux in zero external field) form due to thermal fluctuations above the lowest-energy Meissner state. Entropic considerations lead to the unbinding of the vortex/antivortex pairs at a characteristic temperature T_{2D}, defined implicitly by the equation

$$k_B T_{2D} = \frac{\phi_0^2}{8\pi \mu_0} \frac{d}{\lambda^2(T_{2D})}, \qquad (1)$$

where ϕ_0 is the flux quantum, μ_0 the permeability of free space, d the thickness of the film, and $\lambda(T_{2D})$ the *ab*-plane magnetic penetration depth. Evidence of this vortex unbinding transition has been seen in both resistivity studies as well as superfluid density measurements [1,6] for various superconducting films. For superfluid density, the appearance of free vortices and antivortices should lead to a near discontinuous change from finite to zero superfluid, while the resistivity should show a sharp rise above T_{2D} of an exponential form, first calculated by Halperin and Nelson [7]. Using the superfluid density as a benchmark for the appearance of vortex/antivortex pairs, a more constrained fit of the Halperin-Nelson theory to the resistivity should be possible. Deviations of the resistivity at higher temperatures from this theory could then be compared and possibly attributed to other fluctuations than vortex phase fluctuations, such as fluctuations in the amplitude of the order parameter.

However, during the course of this study, an unexpected pattern emerged: as T_{2D} decreased, there was an increasingly large temperature region where the superfluid density and resistivity were simultaneously suppressed, complicating the analysis of the vortex fluctuations. Such suppression of the superfluid density has often been associated with sample inhomogeneity. Benfatto and collaborators have done extensive work on how spatially random inhomogeneity can affect the results of the two-coil measurement as well as the measured resistivity, successfully applying this model both to the thin films of BCS superconductors as well as cuprate films [8–12]. Application of this model to our films thereby sheds light on what role spatially random inhomogeneity might play in the suppression of the superfluid density and resistivity, although we find that it fails to adequately explain the experimental data.

II. EXPERIMENT

Our samples are grown via pulsed laser deposition (PLD) using a KrF excimer laser (248 nm). Laser pulses hit a

---

[*]Corresponding author: steers.6@osu.edu

$Ca_{0.3}Y_{0.7}Ba_2Cu_3O_7$ target at a rate of 30 Hz with an energy density of 2.4 J/cm^2 (effective spot size 2.5 mm by 3.0 mm) in an atmosphere of flowing oxygen at 300 mTorr. The films are grown on commercially prepared STO (001) substrates heated to 760 °C, with one unit cell (uc) deposited at a time (1 uc for CaYBCO is 11.8 Å), followed by a 90-s break. A base layer of three uc's of nonsuperconducting $PrBa_2Cu_3O_7$ (PBCO) is deposited between the bare $SrTiO_3$ (STO) and the CaYBCO, and the CaYBCO is capped with 10 uc's of PBCO to protect against degradation. We calibrate the number of laser pulses corresponding to the deposition of a single uc by etching a prepared film of ≈50 to 100 uc's and using AFM to measure the thickness. After deposition, the films are annealed at 450 °C in O_2 pressures ranging from 1 to 650 Torr, which controls the oxygen doping. All samples have the same Ca concentration. Underdoping of the films is accomplished solely through manipulation of the oxygen content during the post-growth annealing.

Back to back measurements of $n_s(T)$ and the resistivity $\rho(T)$ are performed promptly after post-growth annealing to prevent degradation from affecting the results. We achieve temperatures down to 1.3 K through vacuum pumping our cryostats. For the bulk of our samples, film resistance is measured by the standard dc four-point technique in the Van der Pauw geometry. Electrical contact is made through indium pressed directly onto the sample. Although there is occasional contact separation when warming the sample back up to room temperature, the indium generally remains in good contact even with our ultrathin samples. However, to ensure optimal resolution during the superconducting transition, we switched to using a 10-μA, 400-Hz ac current through e-beam evaporated Ag contact pads. This technique is applied in our latest samples.

The superfluid density is measured using a two-coil technique [13]. We place coils of NbTi on either side of the plane of the film and drive one coil with a 50-kHz sine wave. Lock-in amplifiers detect the induced EMF due to the magnetic flux that passes through the other coil, and the mutual inductance of the coils is calculated. When the sample becomes superconducting, some portion of the magnetic field from the drive coil is screened by the film, and the measured mutual inductance drops. If the ab-plane magnetic penetration depth λ is much larger than the film thickness d, as it is for our films, then the induced current density in the film is very nearly uniform through the film thickness. In this case, conductivities of individual layers in the cuprate films add in parallel, and the mutual inductance of the coils is properly related to the complex sheet conductivity $\sigma = \sigma_1 - i\sigma_2$ of the film. λ is defined from $\sigma_2(T)$: $\frac{d}{\lambda^2(T)} \equiv \mu_0\omega\sigma_2(T)$, where ω is the driving frequency [13].

A few thick films (50 uc) were grown and tested for comparison purposes, while the majority of films were either 2, 5, or 10 uc thick. We have grown 10 uc films with T_c's up to 75 K, while we have grown 5 uc films with T_c's up to 60 K and 2 uc films with T_c's up to 40 K. We pause to consider how we should treat the dimensionality of our films. Previous measurements find that the expected drop in superfluid density at the Kosterlitz-Thouless-Berezinskii transition occurs at a temperature consistent with the interpretation that copper-oxide layers are sufficiently coupled that the full film thickness
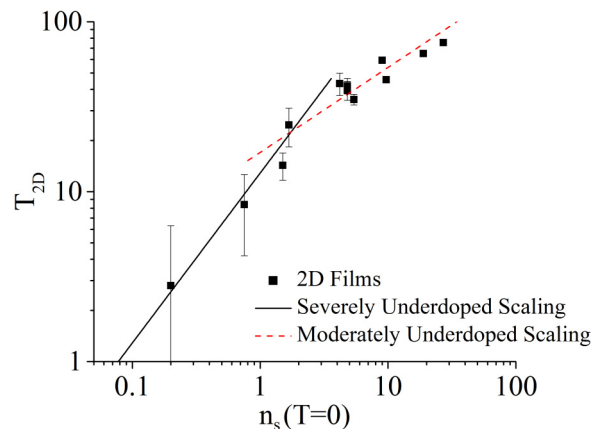

FIG. 1. Scaling between the $T = 0$ K superfluid density and the T_{2D}, confirming the adherence of these films to the scaling observed by Hetel *et al.* [1]. The error bars come from the width of the superfluid transition, while the determination of the expected T_{2D} using Eq. (1) is unambiguous.

behaves as a single two-dimensional film [14]. This is puzzling from a theoretical side, for at $T = 0$, the c-axis coherence length for YBCO, ξ, is approximately 4 Å, less than the c-axis unit-cell dimension of 11.8 Å. One could postulate that ξ grows with temperature until it exceeds the film size, but we suspend theoretical discussion of ξ and instead rely upon the experimental phenomenology to justify treating the films as 2D. The fact that the film thickness values in this study are at least an order of magnitude less than the ab-plane penetration depth λ further supports this view. The diamagnetic currents set up in response to a magnetic field will be uniform through the thickness of the film. Although in bulk cuprates the presence of multiple independent layers can modify the vortex/antivortex interactions from the pure 2D case [15], there are so few layers in our films that the vortex/antivortex interaction is not substantially altered. From these considerations we conclude that films of up to and including 10 uc's such as in this study are adequate approximations to 2D, as will be further discussed during the analysis of the data. This adequacy is further supported by the adherence of severely underdoped films to the 2D scaling found by Hetel *et al.* [1], shown in Fig. 1. The Appendix contains all superfluid and resistivity data for the 2D films used in this study.

III. RESULTS

Figure 2 shows the superfluid density and resistivity ρ in the vicinity of the transition to superconductivity for a film that is 50 unit cells thick, totaling 59 nm. For our purposes, this is a thick film [14]. As one would expect from crystals and other studies on "thick" (20 to 100 uc) films, the resistive and superfluid transitions are fairly close in temperature. Defining $\delta T_c = T_c^\rho - T_{2D}$, where T_c^ρ is the temperature during the superconducting transition such that the resistance has dropped to $\frac{1}{10}$ of the normal state value, we have $\delta T_c = 0.9$ K. As cuprates generally have non-negligible transition width, the few-K difference between the transitions is well explained by the use of the 10% point of the resistive transition for our resistive critical temperature. The resistance can be seen to
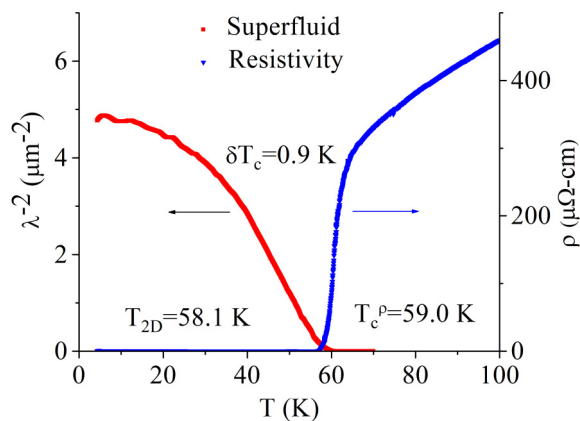
FIG. 2. Superfluid density and resistivity for a thick (50 uc) CaYBCO film (sample 121116). The offset δT_c (defined in the text), resistive critical temperature T_c^ρ, and the 2D vortex unbinding temperature T_{2D} are labeled on the graph. δT_c is seen to be relatively small, i.e., T_c^ρ and T_{2D} are comparable.

drop to zero at the same temperature as the appearance of superfluid density.

Contrary to expectations from thick films, two-dimensional films show a large temperature region where both the superfluid and the resistance are suppressed. Figure 3 shows the resistivity and superfluid measurements for an archetypal film of 5 uc thickness. The opening of a large offset δT_c is immediately apparent upon visual inspection even before any quantitative analysis is performed. δT_c is more than $\frac{1}{3}$ of both T_c^ρ and T_{2D}.

We plot δT_c versus T_{2D} in Fig. 4. The offset clearly decreases with increasing 2D temperature in a linear fashion. We emphasize that this behavior is seen over nearly two orders of magnitude in temperature. Several films even showed a resistive transition while the superfluid response remained zero down to the experimental lower limit of 1.3 K. We took these films to have $T_{2D} = 0$. This leads one to ask whether a whole range of T_c^ρ might be possible at $T_{2D} = 0$. Current work focuses on creating and measuring films with resistive transitions near 0 K. Although initial results indicate that such films are possible, we have not yet systematically explored this
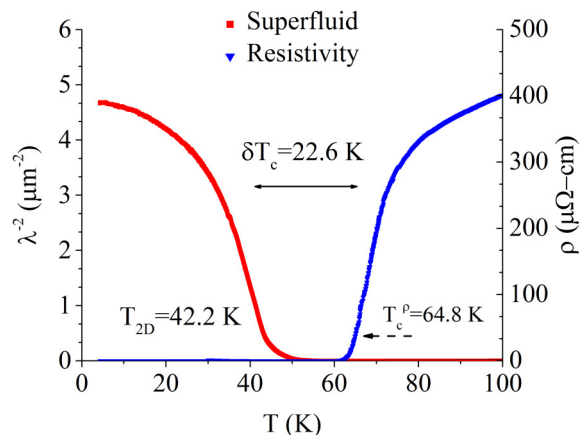

FIG. 3. Superfluid density and resistivity for a 5 uc CaYBCO film (sample 120807). The large temperature region where both responses are suppressed is quantified by $\delta T_c = T_c^\rho - T_{2D}$.
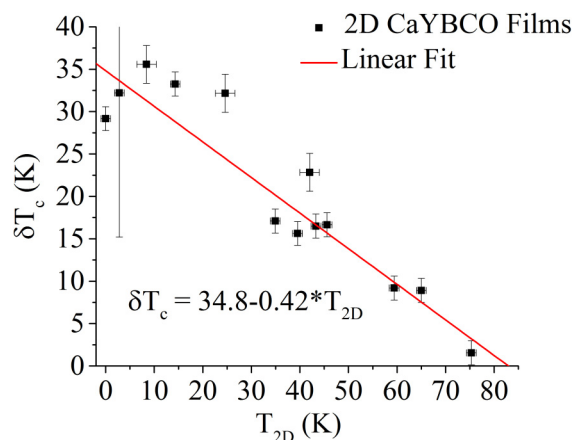

FIG. 4. Critical temperature offset δT_c versus vortex unbinding temperature T_{2D} for several two-dimensional Ca-doped YBCO films. The red line is a linear fit to the data. Error bars arise from the determination of T_{2D} and T_c^ρ.

region of the phase diagram, and as such we do not include the data here. The exact definition of the offset does not affect the order of magnitude of the offset nor the increase of the offset with underdoping. To illustrate this point, Fig. 5 presents the offset defined using $T_{ns}^{1\%}$, the temperature where the superfluid has dropped to 1% of the its $T = 0$ K value, in place of T_{2D}. Although there is a slightly larger scatter in the data than for the T_{2D} offset, the increase with underdoping is clear.

Figures 6–8 show closeups of the offset region for several films. In Fig. 6, we see that for large T_{2D}, the superfluid and resistivity, although largely suppressed, are still non-negligible, and meet at 75.95 K. At the moderate T_{2D} in Fig. 7, we again see that the superfluid density and resistivity meet at a given temperature, although each is suppressed over several K by three orders of magnitude from its bulk-state value. Finally, at the even lower T_{2D} in Fig. 8, there is a clear temperature region where the superfluid density and resistivity have dropped below our experimental resolution.
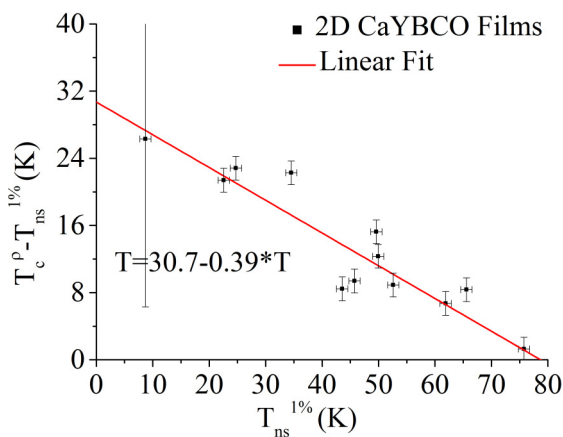

FIG. 5. Critical temperature offset δT_c versus the temperature $T_{ns}^{1\%}$ where the superfluid has dropped to 1% of its $T = 0$ K value for several two-dimensional Ca-doped YBCO films. The red line is a linear fit to the data. Error bars arise from the determination of $T_{ns}^{1\%}$ and T_c^ρ.
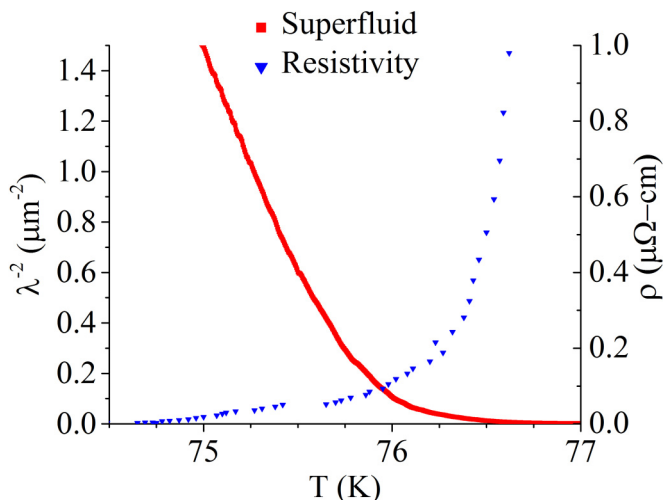
FIG. 6. The transition region for film 120509, which has a large value for $T_{2D} = 75.3$ K, with both λ^{-2} and ρ below the levels defining their respective critical temperatures. $T_c^\rho = 77.1$ K. Note how there is a nonzero temperature region where λ^{-2} and ρ are both nonzero.

FIG. 8. A closeup in the transition region for the film 120724, with a moderately low value of $T_{2D} = 24.6$ K. $T_c^\rho = 56.8$ K. Both λ^{-2} and ρ are suppressed to below experimental resolution over a significant temperature range. Between 44 and 46 K, a temperature-independent voltage offset has been subtracted from ρ corresponding to $0.06 \, \mu\Omega$ cm. Below 44 K, a weakly temperature-dependent voltage of $0.03 \, \mu\Omega$ cm/K, attributed to thermal emf, has been subtracted.

While the offset increases with underdoping, the resistive transition becomes wider. The width is defined by locating the temperature, denoted $T^{100\%}$, where the resistance begins to show a precipitous change in curvature with decreasing temperature and then locating the temperature range over which the resistance achieves 90% and 10% of its value at $T^{100\%}$. These points are shown in Fig. 9. Figure 10 shows the width of the resistive transition plotted against T_{2D} for the respective film. It is important to note that although the resistive transition broadens with underdoping, the superfluid response still occurs at a temperature far less than where the resistance is significantly suppressed, in some films by five orders of magnitude below the normal-state resistance. Extended regions of significant resistivity do not eliminate the increase in the offset with underdoping.

The resistive widening is mirrored by the real part of the sheet conductivity $\sigma_1(T)$. σ_1 constitutes the dissipative portion of the film response to a magnetic field, and generally
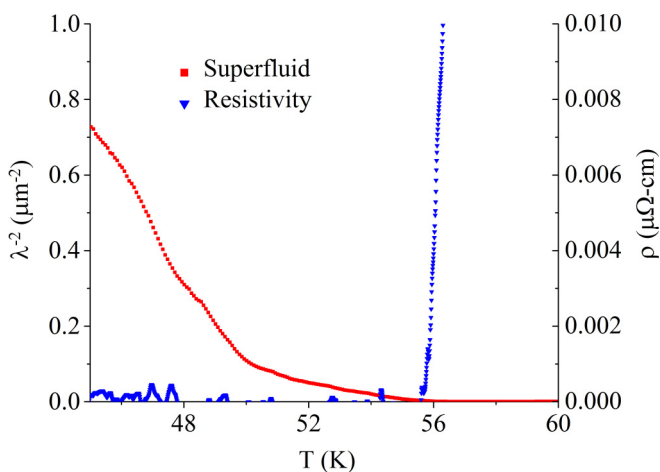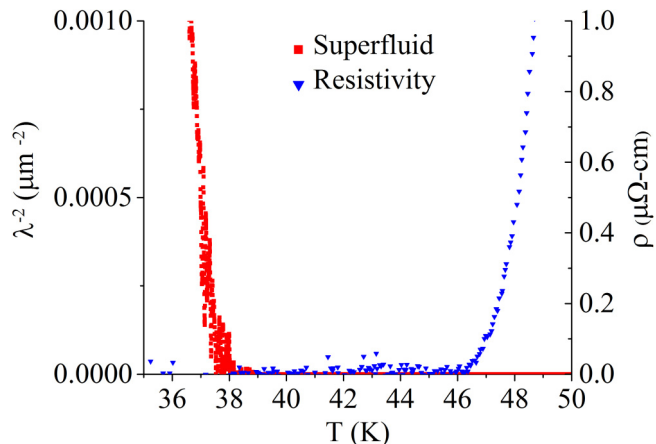
exhibits a peak at a temperature $T_{\max \sigma_1}$ that is within a few Kelvin of T_{2D}. Thus, σ_1 is generally associated with thermally excited vortices. The width of the peak has traditionally been taken as a mixture of film homogeneity and intrinsic physical effects, with a smaller full width at half maximum (FWHM) indicating a more homogeneous film [2]. Figure 11 plots the FWHM of $\sigma_1(T)$ versus $T_{\max \sigma_1}$. The FWHM of the peak in σ_1 is generally largest at severe underdoping, and decreases as $T_{\max \sigma_1}$ attains larger values (which can be associated with higher T_{2D}). Although this may suggest itself as the source of the offset, closer examination reveals that when σ_1 has a larger FWHM, the peak in σ_1 is often not symmetric about $T_{\max \sigma_1}$. Rather, $T_{\max \sigma_1}$ tends to occur closer to the higher-temperature end of the superfluid transition, while shoulders in the lower-temperature side of σ_1 inflate the FWHM. An example of this can be seen in Fig. 12, showing σ_1 for the 5 uc film 120807. We expect that this shoulder

FIG. 7. The transition region for the film 151020, with a moderate value of $T_{2D} = 43.3$ K. $T_c^\rho = 62.5$ K. λ^{-2} and ρ go to zero at the same temperature.
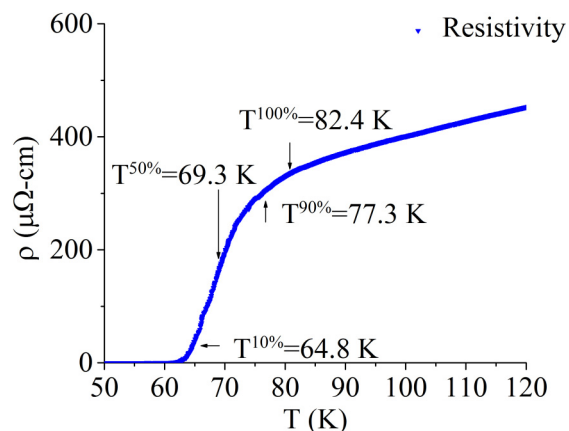

FIG. 9. The resistivity for the 5 uc film 120807 showing the positions that define $T^{100\%}$, $T^{90\%}$, $T^{50\%}$, and $T^{10\%}$, as used in determining T_c^ρ and the width of the transition.
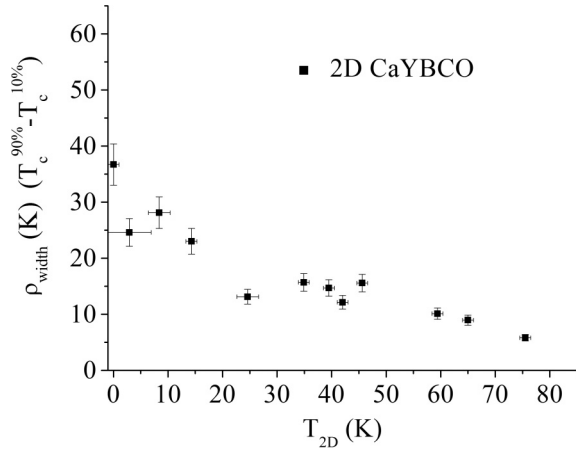
FIG. 10. The width of the resistive transition, defined as $T^{90\%} - T^{10\%}$, versus T_{2D}. A strong dependence on T_{2D} can be seen, suggesting a connection between how readily thermal vortices unbind and the widening of the resistive transition. Error bars are based upon the error in determination of the defining temperatures.

in σ_1 corresponds to a minority, yet nontrivial, percentage of the film transitioning into the vortex state, and thereby yielding dissipation. Since the appearance of these nonsuperconducting regions does not correspond to a significant decrease in n_s, we infer that n_s rapidly decreases only when a majority of the film has entered the nonsuperconducting state. Since this downturn is precisely what happens at T_{2D}, only a minority of an inhomogeneous film would be in the superconducting state in the offset region, i.e., that temperature region above T_{2D}. This adds to our skepticism that the simultaneous suppression of n_s and ρ is an artifact of inhomogeneity.

The appearance of the offset in ultrathin CaYBCO films naturally aroused our curiosity as to ultrathin $Bi_2Sr_2Ca_1Cu_2O_8$ (BSCCO). Much to our surprise, a 200 nm (65 uc) BSCCO film showed a significant offset (see Fig. 13). Thin BSCCO films (4 to 10 uc) similarly showed an offset. Systematic study of the offset in ultrathin BSCCO is in order, although controlling film homogeneity is less advanced than in ultrathin CaYBCO.
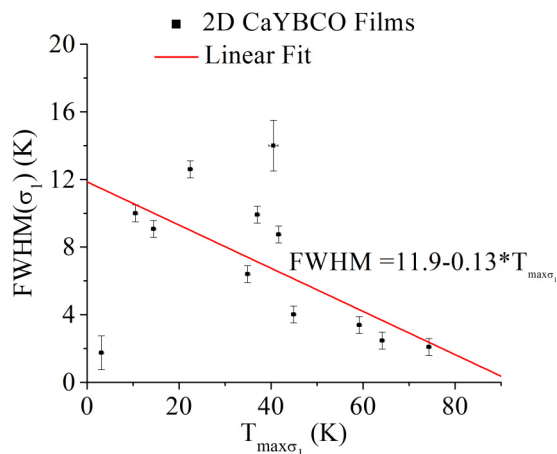

FIG. 11. The full width at half maximum of $\sigma_1(T)$ versus the location of the peak in σ_1 for the films presented in this paper. There is a general linear trend, with narrower peaks at higher temperatures.
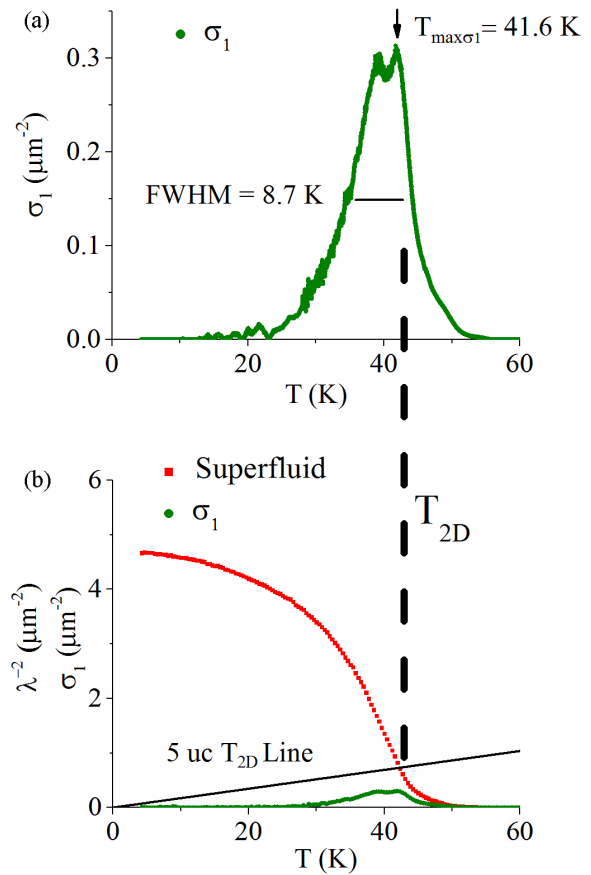

FIG. 12. (a) σ_1 for the 5 uc film 120807, with $T_{\max \sigma_1} = 41.6$ K. σ_1 is clearly not symmetric about this temperature. Even if the midpoint between the cusps is chosen to define $T_{\max \sigma_1}$, the peak is not symmetric. (b) σ_1 compared against $n_s = \lambda^{-2}(T)$. Despite the shoulder in σ_1 at temperatures below $T_{\max \sigma_1}$, n_s drops below $\frac{1}{10}$ of its $T = 0$ value when σ_1 peaks.

IV. ANALYSIS

A. Fits of fluctuation effects

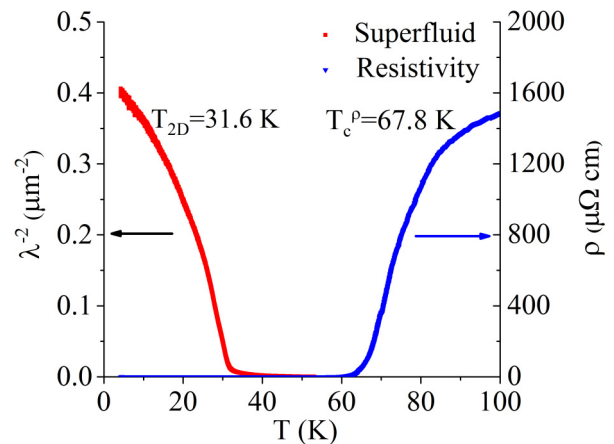We start our quantitative analysis with the superfluid density. Figure 14 shows the superfluid density data for

FIG. 13. A 65 uc (200 nm) BSCCO film, showing the same offset behavior as ultrathin CaYBCO films.
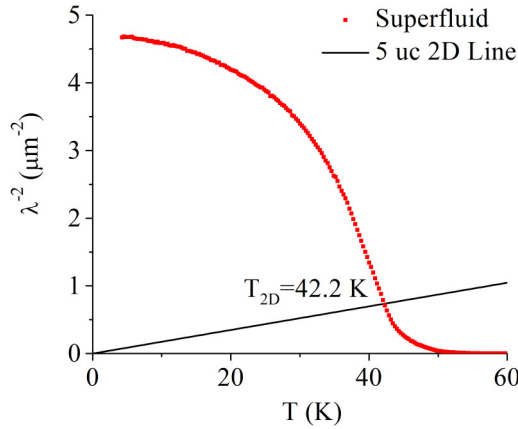
FIG. 14. Superfluid density λ^{-2} for the 5 uc film 120807. The intersection of the line labeled "5 uc KTB line" with λ^{-2} determines T_{2D}.

the 5 uc film 120807 as well as the T_{2D} line, constructed from Eq. (1) so that the intersection of $\lambda^{-2}(T)$ and the T_{2D} line gives the expected value of T_{2D}. In our experiment, the determination of T_{2D} is unambiguous, as $\frac{d}{\lambda^2}$ is extracted directly from the measured mutual inductance [13], while ϕ_0, μ_0, and k_B are constants. Hence, errors in measurements of other film properties, such as thickness d, do not affect T_{2D}, given that the CuO planes of CaYBCO have been found to be coupled rather than independent [2]. Further information is extracted from the superfluid density by taking a quadratic fit to the low-temperature data, motivated by the expected $\lambda^{-2}(T)$ dependence for a dirty-limit d-wave superconductor [16], with 3D films of CaYBCO showing good agreement to the d-wave form to within a few K of T_c [17]. The zero of the quadratic fit could be interpreted as T_c^{mf}, the mean field transition temperature in the absence of fluctuation effects. The right panels of the figures in the Appendix, Figs. 25–36, show the low-temperature fit in comparison to the resistivity. Although for some curves the quadratic fit goes to zero reasonably close to the resistive transition, other films, such as the 5 uc film 120724 shown in Fig. 15, show a greater discrepancy. Clearly, identifying the zero of the fit as T_c^{mf} is problematic. Whether
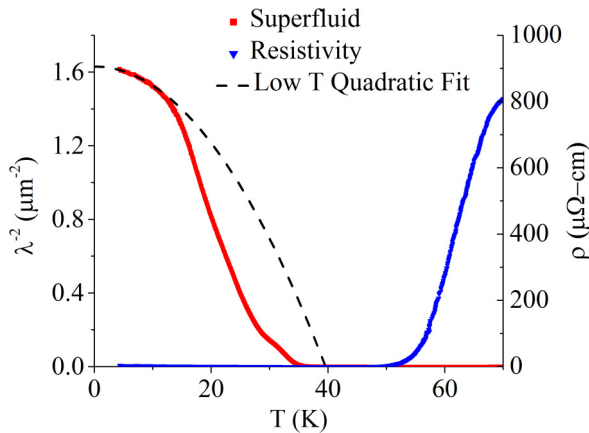

FIG. 15. Quadratic low-temperature fit to the superfluid density of the 5 uc film 120724. The zero of the fit falls far short of the resistive transition.

this stems from the same source as the offset δT_c or is due to the general inapplicability of the quadratic form at higher temperatures for our 2D films is unclear. The fit also helps determine $n_s(0)$, which is used to confirm that the film conforms to the expected linear scaling between T_{2D} and $n_s(0)$ [1].

The analysis of the resistivity begins by separating out the contributions from the PBCO buffer layers and the CaYBCO layers. The contribution of the PBCO buffer layers is modeled by variable range hopping (VRH) conductivity taken from the literature [18,19]. The same VRH parameters are used regardless of the doping. Due to the ultrathin nature of our CaYBCO, the PBCO conductivity can have a sizable contribution at higher temperatures, especially for severely underdoped CaYBCO, accounting for up to 10% of the measured resistivity at room temperature. However, this contribution is less important in the temperature range where the transition occurs, especially as the increased conductivity of the superconducting state comes to dominate the total conductivity of the film. Consequently, the resistivity near the transition is presented without adjustment for the contribution from PBCO.

We take a simple linear fit as a first-order approximation for the in-plane normal-state resistance given the work of Wuyts, Moshchalkov, and Bruynseraede [20]. The resistive transition itself is modeled using two-dimensional Aslamazov-Larkin (AL) corrections to the normal-state conductivity

$$\sigma_{AL} = \frac{e^2}{16\hbar d \ln \epsilon}, \tag{2}$$

where $\epsilon = \frac{T}{T_c^{AL}}$ and d is a relevant thickness scale. For completeness we will compare fits using both the single unit-cell thickness and the full film thickness for d. The AL corrections represent the formation of Cooper pairs due to thermodynamic fluctuations above T_c. It is mathematically apparent that T_c^{AL} is the critical temperature associated with zero resistance since the conductivity becomes infinite as $T \to T_c^{AL}$ and Cooper pair formation becomes the minimum of the free energy as opposed to a product of thermodynamic fluctuations. We restrict ourselves to the 2D form for uncoupled layers, as the three-dimensional (3D) form is only applicable in about 0.25 K of T_c^ρ, assuming a c-axis coherence length of ≈ 0.4 nm.

For near-optimally doped films, this model gives good agreement with the resistive transition especially at the higher-temperature end, as can be seen in Fig. 16. For severely underdoped films, the agreement is limited to a smaller section of the high-temperature end of the transition. The increasing departure of the normal state from linearity as we approach the SIT is no doubt a factor in this lack of agreement. Figure 16 shows the AL fit for the 5 uc film 120807. We have presented fits using both the single unit cell and the full film thickness as the relevant length scale d. Since the full film thickness governs the vortex/antivortex unbinding transition in the superfluid density [1,2], one would expect that the full film thickness should be used for the AL conductivity. However, a better fit is achieved using the single unit-cell thickness instead. This is not definitive since other effects, including the film inhomogeneity and the deviation of the normal-state resistivity from our simple linear approximation, could be leading to erroneous fits. (It is because of the rather simple linear approximation that we have allowed the normal-state resistivity to differ between
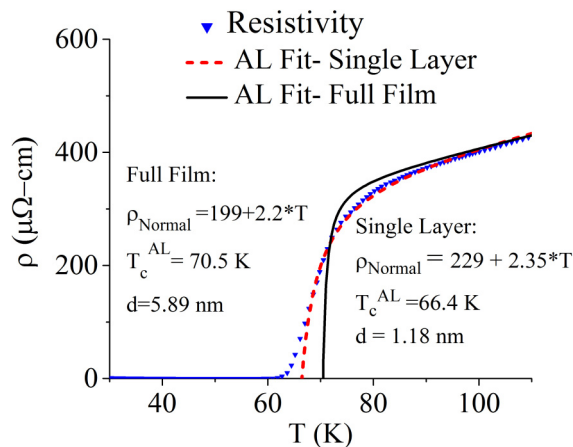
FIG. 16. The 2D Aslamazov-Larkin model for paraconductivity fit to the resistivity of the 5 uc sample 120807 using both a single unit cell and the full film thickness as the relevant thickness scales. We have assumed a normal-state resistivity linear in temperature and allowed it to vary between the two fits. The fit for using a single unit cell is in reasonable agreement for the upper half of the transition, while the resistivity changes curvature at lower temperatures, deviating from the fit. The AL fit for the full film thickness deviates greatly from the data, but as explained in the main text, the quality of this fit as well as the single-layer fit could be happenstance arising from other effects.

the two fits, and have not held the normal-state temperature dependence to be rigidly fixed.) These effects would have to be rigorously accounted for before one could say that the copper oxide layers are decoupled during the resistive transition.

Turning to the low-temperature end of the resistive transition, we attempt to apply the model of Halperin and Nelson (HN) [7]. Thermally excited vortices and antivortices, having opposite magnetic moments, will move in opposite directions under the influence of a dc electric current. When the vortex/antivortex pairs are bound, these opposite responses result in no net motion for the pair, but at T_{2D}, the vortices and antivortices should begin to move, resulting in an induced electric field opposite to the supercurrent flow. This electric field causes dissipation, and the sample should exhibit a voltage dependent upon the number of vortices and antivortices present. Halperin and Nelson calculated this resistance:

$$\frac{R_\square}{R_{N\square}} = C \exp\left(-2b\sqrt{\frac{T_c - T_{2D}}{T - T_{2D}}}\right), \quad (3)$$

where $R_{N\square}$ is the normal-state sheet resistance, T_c is the mean field transition temperature, and C and b are constants of order unity [6,7]. As a phenomenological choice, we take T_c to be $\approx T_c^\rho$, the measured resistive transition temperature, allowing a less than 2-K variation for goodness of fit. Figure 17 shows this model applied to the 5 uc film 120807, determined by seeking linear regions in $\ln\rho$ versus $(T - T_{2D})^{-0.5}$. This is shown in Fig. 18, revealing approximately three linear regions in $T - 42.2$ K that correspond roughly to the very low-temperature end of the transition, the first 10% of the transition, and the high-temperature end of the transition.

In each of these temperature regimes, the model of HN can be made to fit the data by altering the fitting parameters, yet
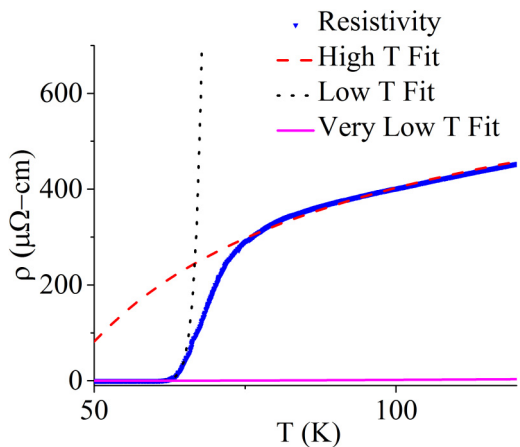

FIG. 17. Fits of the Halperin-Nelson theory for resistance due to thermally excited vortices to the 5 uc film 120807 resistivity, as extracted in Fig. 18. $T_{2D} = 42.2$ K. By altering some of the fitting parameters, the theory can be made to replicate specific temperature regions of the resistivity, but fails to provide a logically consistent fit.

it greatly deviates from the resistivity curve outside of those temperature regimes. At the very low end of the transition, the fitting procedure yields a fit only to the lowest resistivity values. As it misses almost the entirety of the transition, as well as fitting those ultralow resistivity values most affected by experimental noise, this fit is obviously unreasonable. At the high-temperature end, the fit is again unreasonable, as it misses the rapidity with which the resistivity falls with decreasing temperature. Furthermore, the very applicability of HN to the high-temperature end is unsound, as it is expected that the HN model should give way to AL fluctuations [11]. Near $T^{10\%}$, a decent agreement is achieved in the region where the HN form is expected to be applicable, but with grossly inappropriate fitting parameters, namely, $C = 2.75 \times 10^{19}$ and
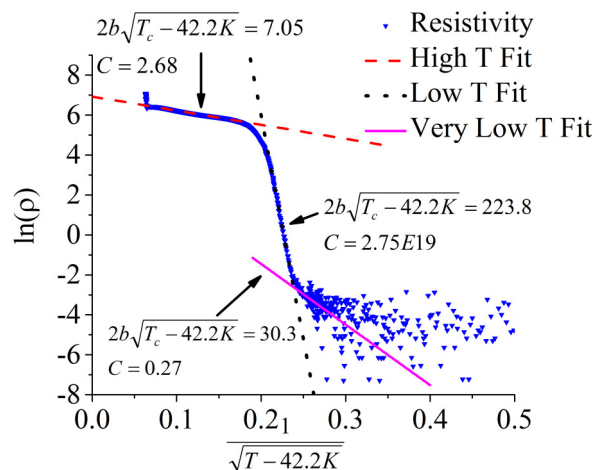

FIG. 18. First method of fitting the Halperin-Nelson theory (dashed line) for resistance due to thermally excited vortices to the 5 uc film 120807 resistivity. The natural log of the resistivity is plotted against the argument of the exponent in the Halperin-Nelson resistivity [Eq. (3)]. Three linear regions that might fit the theory are extracted. Here, $T_{2D} = 42.2$ K, taken from the superfluid data, while the values for b and T_c are left free since this fitting procedure only fixes their functional relationship.
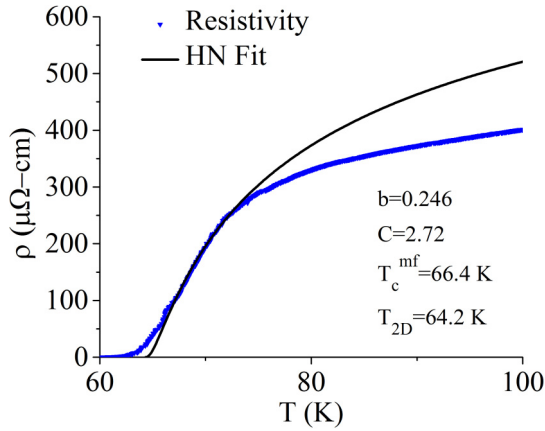
FIG. 19. Halperin-Nelson fit to the resistivity of the 5 uc CaY-BCO film 120807 leaving T_{2D} as a free parameter. This yields a value of $T_{2D} = 64.2$ K, much higher than the $T_{2D} = 42.2$ K derived from λ^{-2}. The fitting parameters are far more reasonable than when using the lower value of T_{2D}.

$b \approx 20$, assuming T_c is somewhere between 60 and 80 K. The prime culprit in this appears to be the extremely low value of T_{2D}. To give even a remotely useful fit to the data, any parameter selection should at least yield a low value for ρ below the transition, and cross the resistivity data at one point. If we require $\rho(60 \text{ K}) \leqslant 1 \ \mu\Omega\text{ cm}$ and $\rho(78 \ K) = 320 \mu\Omega\text{ cm}$, b must exceed 16, while $C > 10^9$ for any choice of T_c^{mf} between 60 and 80 K. If we instead take T_{2D} as a free parameter, and attempt to fit the data directly, we achieve more reasonable results, but are then still faced with a significant discrepancy between T_{2D} from the superfluid and resistive data. Figure 19 shows an example of this fit for the 5 uc film 120807. The fit yields $C = 2.72$ and $b = 0.246$, but using $T_{2D} = 64.2$ K, which is decently higher than the value of 42.2 K obtained from the superfluid data. The HN fit is compared to the single-layer AL fit in Fig. 20. As expected, the HN model gives a better
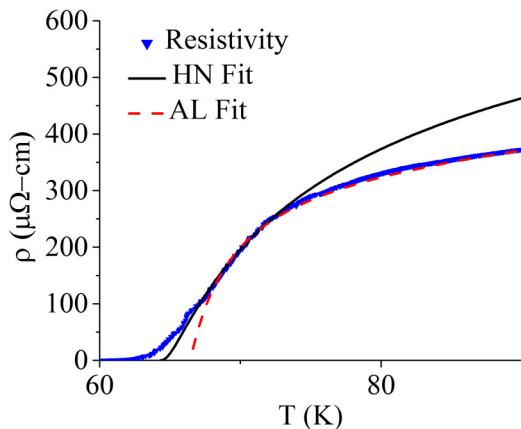

FIG. 20. Halperin-Nelson fit to the resistivity of the 5 uc CaY-BCO film 120807 leaving T_{2D} as a free parameter compared with the 2 uc This yields a value of $T_{2D} = 64.2$ K, much higher than the $T_{2D} = 42.2$ K derived from λ^{-2}. The fitting parameters are far more reasonable than when using the lower value of T_{2D} extracted from the superfluid density transition.

fit at the low-temperature end of the transition, while the AL model gives a better fit at the high-temperature end.

B. Analysis of film inhomogeneity

Although in some films the superfluid density shows a sudden downturn in the vicinity of T_{2D}, as expected, other films have a more rounded, broad transition. There is also a small tail at upper temperatures. Given that this tail is mirrored in the resistivity, as well as the sizable widths of both σ_1 and ρ, it would seem that there is a less than desirable amount of inhomogeneity in several of our films. It has been pointed out that inhomogeneity can lead to erroneous fitting values when attempting to apply HN and AL models of the resistivity [11]. Inhomogeneity could certainly be causing some of the issues with the fits of the previous section, such as the deviation of the HN fit at low temperatures from the measured resistivity (see Fig. 19). This naturally raises the question of how inhomogeneity might relate to the offset.

To answer that question, we applied the renormalization group (RG) analysis of Ref. [21] to one of our films. In that work, Benfatto *et al.* derive RG flow equations appropriate for 2 unit-cell CaYBCO films undergoing the Kosterlitz-Thouless-Berezinskii 2D vortex/antivortex unbinding transition mentioned in the Introduction. Using the low-temperature quadratic fit $\lambda^{-2}(T = 0) - \alpha T^2$ (where α is a constant) as the superfluid density in the absence of vortex/antivortex pairs, the RG equations can be numerically solved to yield a renormalized $\lambda^{-2}(T)$. For a perfectly homogeneous film, the only fitting parameters for this procedure would then be the coupling between the layers of the film and the vortex creation energy μ. We follow Benfatto *et al.* in keeping the initial interlayer coupling a constant fraction of the superfluid stiffness (which is proportional to λ^{-2}). As for μ, it is selected so that the RG calculated transition occurs at the same temperature as the experimental data. In practice, this was selected to be near T_{2D}, which also generally agreed with the peak in σ_1. For an inhomogeneous film, the procedure can be repeated using different values of $\lambda^{-2}(T = 0)$, and the total superfluid response of the film fit by assuming that the film consists of regions with a local value of $\lambda^{-2}(T = 0)$. These regions are taken to be randomly distributed in space, occurring with Gaussian probability. Averaging the calculated renormalized superfluid curves over the Gaussian distribution then provides a fit to the experimental data. As we were able to reproduce the curves in Ref. [21], we are confident that we are properly applying the methodology to our samples.

Figure 21 shows the superfluid fit for the 2 uc film 120802. The bulk of the curve can be fit with a single Gaussian. However, to achieve the tail at the higher-temperature end of the transition, we added a second Gaussian distribution with a small weighting compared to the first. Consequently, the probability distribution $P[\lambda^{-2}(T = 0)]$ was

$$\frac{P_a}{\sqrt{2\pi\sigma_a^2}}e^{-\frac{(\lambda^{-2}-\overline{\lambda_a^{-2}})^2}{2\sigma_a^2}} + \frac{P_b}{\sqrt{2\pi\sigma_b^2}}e^{-\frac{(\lambda^{-2}-\overline{\lambda_b^{-2}})^2}{2\sigma_b^2}} \qquad (4)$$

with $P_a = 0.982$, $\overline{\lambda_a^{-2}} = 1.438 \ \mu\text{m}^{-2}$, $\sigma_a = 0.489 \ \mu\text{m}^{-2}$, $P_b = 0.018$, $\overline{\lambda_b^{-2}} = 3.121 \ \mu\text{m}^{-2}$, and $\sigma_b = 0.624 \ \mu\text{m}^{-2}$. The
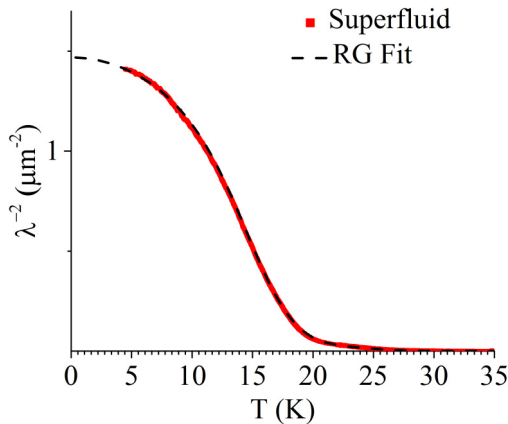
FIG. 21. Fit of the superfluid density for the 2 uc film 120802 accounting for inhomogeneity. Most of the transition could be captured using a single Gaussian probability distribution for the local superfluid densities. The tail at high temperature required a small contribution from a second Gaussian.
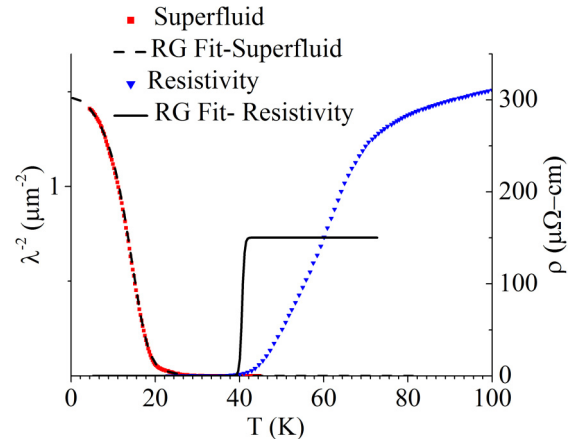

FIG. 22. The resistivity calculated from the RG analysis of film 120802. Despite a number of approximations erring on the side of lower resistivity, the calculated resistivity still rises much more quickly than the experimental resistivity.

value for μ, in units of the vortex energy expected from the XY model, was 2.02, which is within 6% of the value reported in Ref. [21] for films with comparable T_{2D}, further supporting the applicability of this RG approach to our particular samples.

Once the RG calculations have accounted for the inhomogeneity in λ^{-2}, the same equations can provide insight into the resistive transition by extracting the vortex correlation length ξ (not to be confused with the coherence length) and converting it into a resistance in the manner of Refs. [9,11]. A full treatment of the resistivity would extrapolate from the result of the RG calculation to include the effects of AL fluctuations near and above T_c^{mf}, which in this case corresponds to the zero of the low-temperature quadratic fit used for the bare superfluid density. An effective medium theory (EMT) would then be used to calculate the resistivity resulting from the randomly distributed local values of $\lambda^{-2}(T=0)$, the probability distribution of which has already been calculated in reference to the superfluid density data. This is beyond the scope of this paper. We need only consider what the minimum resistivity might be for a film with a spatially random distribution of superfluid transitions, with concomitant $\rho(T)$ curves. As the resistivity that can be calculated from the vortex/antivortex RG equations is capped at $0.5R_N$ [11], while the major effect of AL fluctuations would be to suppress R_N to between 1 and 0.5 except for a small region around T_c^{mf}, we take the resistivity calculated from the RG analysis as is. On the whole, we believe this to be a reasonable approximation considering that we need not exactly replicate the resistivity data, but rather ascertain if spatially random inhomogeneity can account for the offset. In the same vein, we do not perform an EMT analysis, but rather take all the local resistivities to be in parallel. This represents the lowest possible resistivity that such a collection of resistors can assume. As even one superconducting link would completely suppress the resistivity in this scenario, the accuracy of our analysis is limited by numerical considerations, specifically over how many standard deviations we integrate the probability distribution. Care is taken to integrate out to $\lambda^{-2}(T=0)$ values such that higher

values of $\lambda^{-2}(T=0)$ would occur with a probability of less than 1 in 10^9.

Figure 22 shows the calculated resistivity for film 120802. As can readily be seen, the RG calculation produces a resistivity that rises far more rapidly than the observed resistivity. We can only conclude that a spatially random distribution of local superfluid densities cannot account for the offset.

Before leaving the analysis of the experimental data, it is worth noting that we are not the first to experimentally produce the offset in ultrathin CaYBCO films. In his thesis [22], Hetel discusses additional data surrounding the ultrathin CaYBCO films that were used to establish the linear scaling of n_s with T_c at severe underdoping, as presented in Ref. [1]. Among the additional data, Hetel reports both the superfluid density and the resistivity of a single 2 unit-cell sample of CaYBCO (see p. 46 of Ref. [22]). A digitally reproduced copy, along with our determination of T_{2D} and T_c^ρ, is shown in Fig. 23. From these values, we extract $\delta T_c = 11.8$ K, which
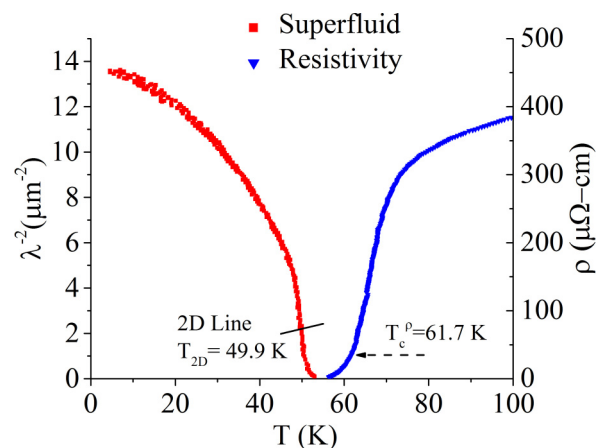

FIG. 23. Superfluid and resistivity data for a 2 uc CaYBCO film reproduced from the thesis of Hetel [22]. The extracted values of T_{2D} and T_c^ρ yield a value of δT_c comparable to the trend line from our samples.
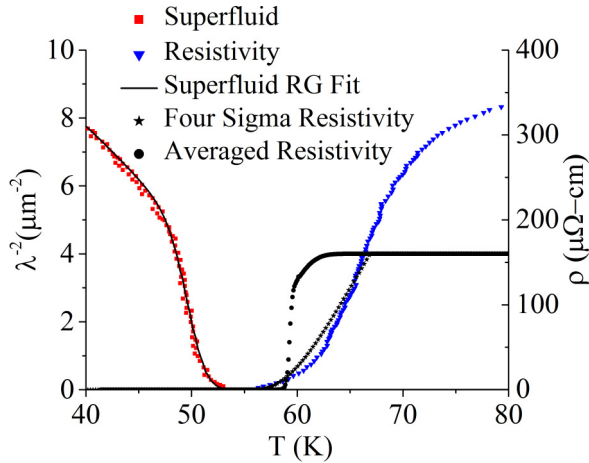
FIG. 24. RG analysis applied to the data from Hetel. The superfluid data are fit using a Gaussian probability distribution for λ^{-2}, with $\overline{\lambda^{-2}} = 13.6$ μm^{-2} and $\sigma = 0.612$ μm^{-2}. The experimental resistivity can be roughly approximated by using only local superfluid values that lie 4σ from the mean. When the total film distribution of superfluid values is taken into account, the calculated resistivity again fails to match the experimental resistivity.

compares favorably with the expected value from our films of $\delta T_c = 34.8$ K $- 0.42 \times T_{2D} = 13.8$ K. Furthermore, when we apply the same RG analysis used earlier to this film, we find that the resistivity would roughly correspond to a T_c $4 \times \sigma$ away from the average T_{2D}, as shown in the expanded view of the offset region in Fig. 24. At $4 \times \sigma$, regions with a higher T_c occur with a probability of only 3×10^{-5}, which would still seem a very small portion of the film to be almost completely determinative of the total film resistivity. When the resistivity of regions lying up to $6 \times \sigma$ from the mean are averaged in parallel, the resistivity clearly rises before the experimental data. Unfortunately, Hetel did not record resistivity data for his severely underdoped films due to difficulties making good electrical contact [22].

V. DISCUSSION

The suppression of both λ^{-2} and the resistivity ρ over an *extended* range in temperature would seem to stretch existing theory if not past its limits, at least to its extreme. To understand the offset, we take as our starting point the superfluid transition. The pronounced downturn of $\lambda^{-2}(T)$ with increasing temperature has been identified with the 2D transition [1,21], and motivates our determination of T_{2D}. The presence of vortices is further supported by the dissipative signal from the two-coil measurement. It would seem clear that thermal vortices unbind at the downturn. As temperature increases, the density of free vortices and antivortices should also increase. When coupled with the dissipative action of vortices, this leads to the Halperin-Nelson form for the resistance below the mean field transition at T_c^{mf} but above T_{2D}. Previous experience, including our own experiments with thick CaYBCO films as in Fig. 2, is that $\frac{T_c^{mf} - T_{2D}}{T_c^{mf}} \ll 1$ [11,23].

Yet, we find that in 2D films, $T_c^{mf} - T_{2D}$ is comparable to T_c^{mf} when we reasonably take $T_c^{mf} = T_c^{\rho}$. Even if T_c^{mf} is taken at some other point on the resistive transition, δT_c is still sizable. More questions are raised if T_c^{mf} cannot be associated with the resistive transition. Thus, it would seem that either a superconducting state with thermal vortices can persist over a larger temperature range than expected, or that some other state or effect interposes between the unbinding of vortices at T_{2D} and the transition to the normal state.

In either case, it is unlikely that the offset is a structural artifact of the films. We would expect structural inhomogeneities, such as defects, impurities, or disordering of the Cu-O chains present in CaYBCO, would be spatially random. Since each structural effect has the potential to lower the local critical temperature, the resulting distribution of local critical temperatures would be spatially random. Yet, the RG analysis explicitly constructed to handle spatially random T_c's failed to account for the offset. A more refined analysis for the resistivity, effective medium theory (EMT), would necessarily fail as well since our weighting of local resistivities represents a lower bound on any EMT resistivity. It is interesting to note that Benfatto *et al.* have explored the applicability of EMT to systems with weak correlation in the spatial distribution of T_c [8] and found reasonable agreement between the EMT calculation and more direct numerical modeling. Thus, any theory of spatial inhomogeneity in the superconducting state that could explain the offset must have a nontrivial degree of spatial correlation.

Any possible link between spatially correlated inhomogeneity and the appearance of the offset would require new physics. One possibility is suggested in Ref. [24], where numerical studies establish that transverse current responses to applied vector fields, normally not present in the BCS model, arise in disordered superconductors. For regions of the film with higher superfluid density, these currents can link neighboring regions to create correlated current paths. A calculation of the extent of this effect for superfluid distributions such as ours would be a useful check on the role of inhomogeneity. In addition, a more exact calculation of the resistivity for our samples, as outlined in the discussion of the RG analysis, might help to clarify the dependence of the offset on T_{2D} by removing the incidental discrepancy due to spatially random inhomogeneity. The RG analysis might be further expanded to include Ref. [25], which would also allow an analysis of σ_1. In that work, σ_1, as measured by two-coil measurements, was found to be anomalously large. This was linked to the slowing down of the vortices, possibly due to inhomogeneity. Given the broad width of our σ_1 curves, further investigations of inhomogeneity are in order.

There is an interesting parallel to be noted between our ultrathin CaYBCO films and measurements on LBCO crystals at $\frac{1}{8}$ doping. In La$_{2-x}$Ba$_x$CuO$_4$ (LBCO) at $\frac{1}{8}$ doping, the c-axis resistive transition occurs at a lower temperature than the ab-plane resistive transition [26]. In the same samples, neutron diffraction shows an enhancement of stripe formation

due to a temperature-induced transition to a low-temperature tetragonal (LTT) state. These stripes are believed to frustrate the interlayer coupling in LBCO, allowing for what are otherwise 2D vortices to have a large impact on the bulk crystal. It has been hypothesized that this temperature effect in the anisotropy of the resistivity is due to a pair density wave (PDW) state, a theoretical electronic state with periodic spatial modulation of the pairing amplitude. The PDW would be a candidate state for linking stripes and superconductivity, and is expected to be more pronounced in 2D systems [27]. LBCO doped to 0.095 exhibits a similar anisotropic phenomenon, but only under nonzero magnetic field, possibly due to differences in stripe formation with doping [28]. Analysis of the form of the c-axis resistivity in these samples suggests that it is due to vortices, which is once again suggestive of our vortex/antivortex physics.

Our CaYBCO films are 2D by construction, and as such already bear a greater resemblance to LBCO samples with interlayer frustration than bulk YBCO, which has fairly strong interlayer coupling. Furthermore, we expect ultrathin CaYBCO films to be tetragonal for two reasons: calcium doping and the use of STO as our substrate. YBCO undergoes a transition from orthorhombic to tetragonal as the oxygen per unit cell decreases below 6.6 [29]. Since partial Ca substitution for Y in YBCO dopes in extra holes, we can readily push the oxygen content of our films below 6.6 while still achieving significant T_c's. Thus, our films will be in a tetragonal state. Furthermore, the underlying STO is cubic in structure, further encouraging tetragonal rather than orthorhombic film formation. Coupled with the temperature separation between the appearance of vortices in our superfluid density measurements and the ab-plane resistivity, the possibility that ultrathin CaYBCO is also a candidate for a PDW demands further experimental investigation. We hope to test thin LBCO films at $\frac{1}{8}$ doping to further establish the connection between LBCO and ultrathin CaYBCO.

If the offset is indeed indirect evidence for a PDW, ultrathin CaYBCO would be an excellent test bed for models probing the energy scales associated with a PDW. In LBCO, observation of the zero magnetic field offset requires strong stripes to make the sample 2D and thus limits the doping range over which it can be easily observed. Ultrathin CaYBCO is 2D by construction, and thus does not require strong magnetic fields to produce the offset. Given that doping in CaYBCO can be continuously controlled through post-growth annealing, a heightened level of model parameter control can be achieved that is rare in solid-state systems.

The appearance of an offset in thick BSCCO films is at first surprising, but on further examination fits within a picture of a 3D versus a 2D QCP as a factor in the offset. Previous work has shown that 2D and 3D CaYBCO films obey different scaling relationships for T_{2D} and $n_s(0)$ [1,2], corresponding to the expected scaling difference between a 2D and 3D QCP. This is logically consistent with the appearance of the offset in 2D films but not in 3D films of CaYBCO. BSCCO is more anisotropic than YBCO, and 2D features appear to persist in otherwise thick films. Thick films ($\approx$60 uc) of BSCCO

show the same 2D linear scaling of $\lambda^{-2}(0)$ with T_c as ultrathin YBCO [16], while more homogeneous 10 uc films show the *same* quantitative relationship as YBCO over and above the equivalence of the scaling form [30]. Further investigation of BSCCO is in order, especially as regards the role of dimensionality and inhomogeneity in driving the formation of any offset.

VI. CONCLUSION

We have measured a temperature regime in ultrathin films of Ca-doped YBCO showing simultaneous suppression of the resistance and the superfluid density. This "offset" δT_c is a significant fraction of the expected mean field transition temperature associated with the resistive transition T_c^{ρ}. δT_c is linearly dependent upon T_{2D}, the two-dimensional vortex unbinding temperature, and increases upon severe underdoping. The presence of the offset in films that are inherently 2D while its absence in films that respond as 3D, along with doping-dependent features of the offset, are suggestive of the effects of a previously identified 2D quantum critical point in ultrathin CaYBCO [1]. Alternatively, or perhaps complementary, an increased amount of inhomogeneity in films exhibiting a large offset demands a careful analysis beyond naive expectations for the effects of inhomogeneity.

APPENDIX

We show here all superfluid and resistivity data for the films presented in this work. Panel (a) for each film shows the superfluid density (proportional to λ^{-2}), the real part of the sheet conductivity, as well as a quadratic low-temperature fit. Panel (b) for each film shows the superfluid density, the quadratic low-temperature fit, and the resistivity (see Figs. 25–36). Small voltage offsets related to noise and thermal emfs have been subtracted from most resistivity graphs. These were generally small corrections (<1 $\mu\Omega$ cm), except for film 120823. Here, the correction was on the order of the normal-state resistivity. We include the film, although we have ascribed its offset value with correspondingly large error bars. Films 120509, 12217, and 1231 are 10 unit cells thick, films 120604, 120807, 120724, and 120806 are 5 unit cells thick, film 151020 is 4 unit cells thick, and films 120802, Jon's Film, 120803, and 120823 are 2 unit cells thick.
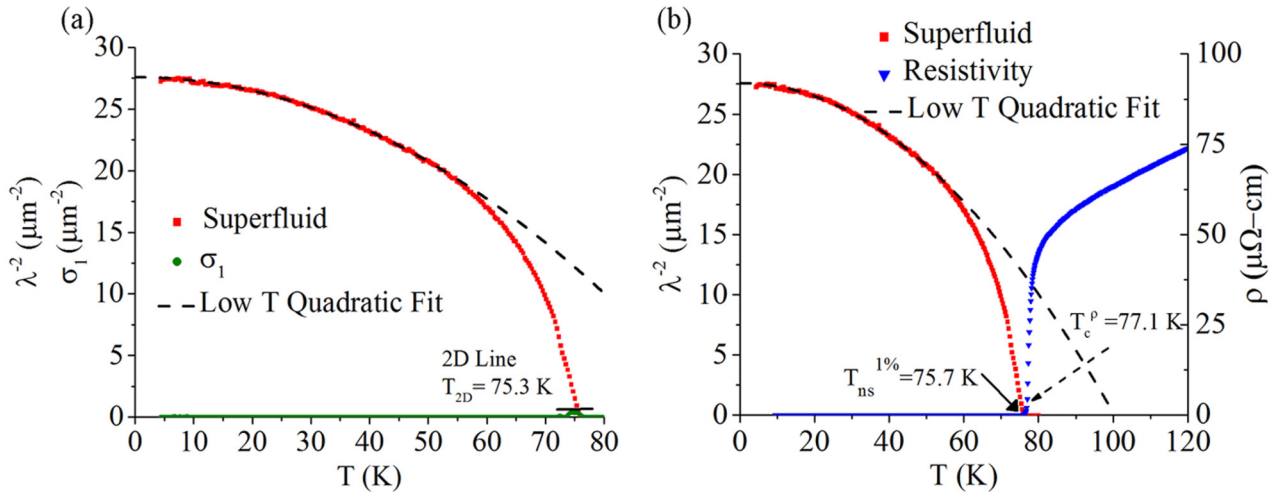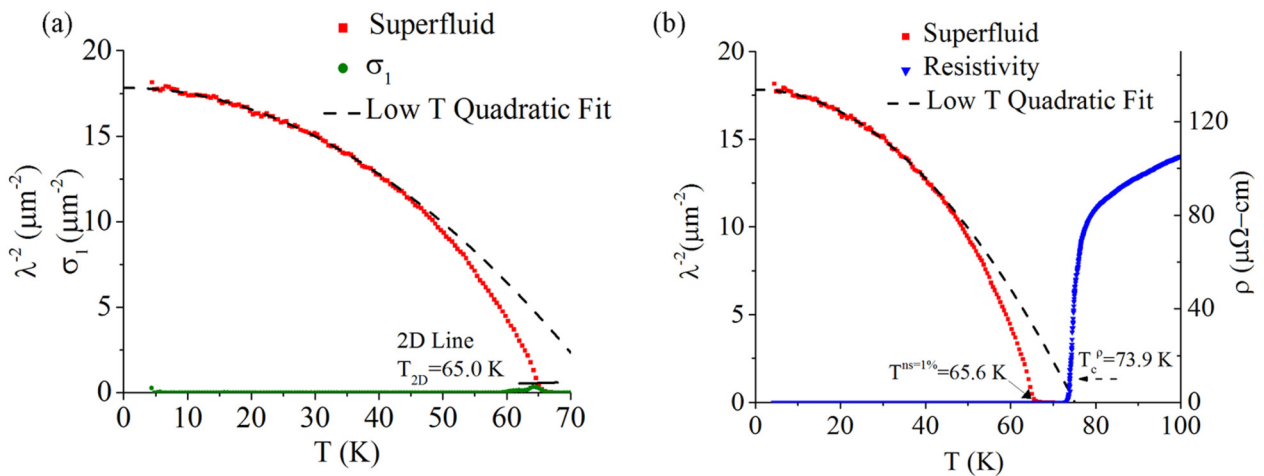
120509

FIG. 25. 10 uc film 120509.

12217
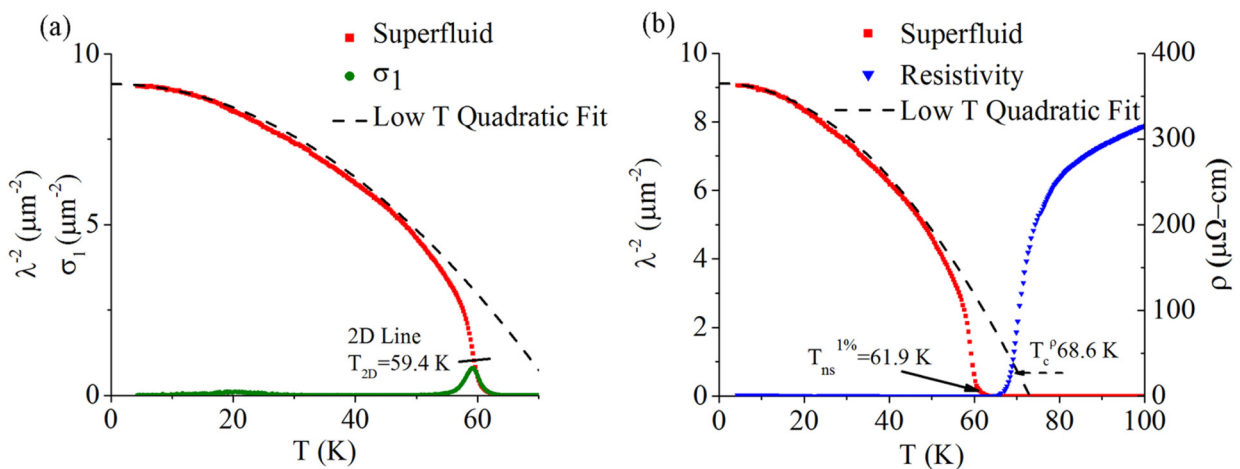

FIG. 26. 10 uc film 12217.

120604

FIG. 27. 5 uc film 120604.

1231

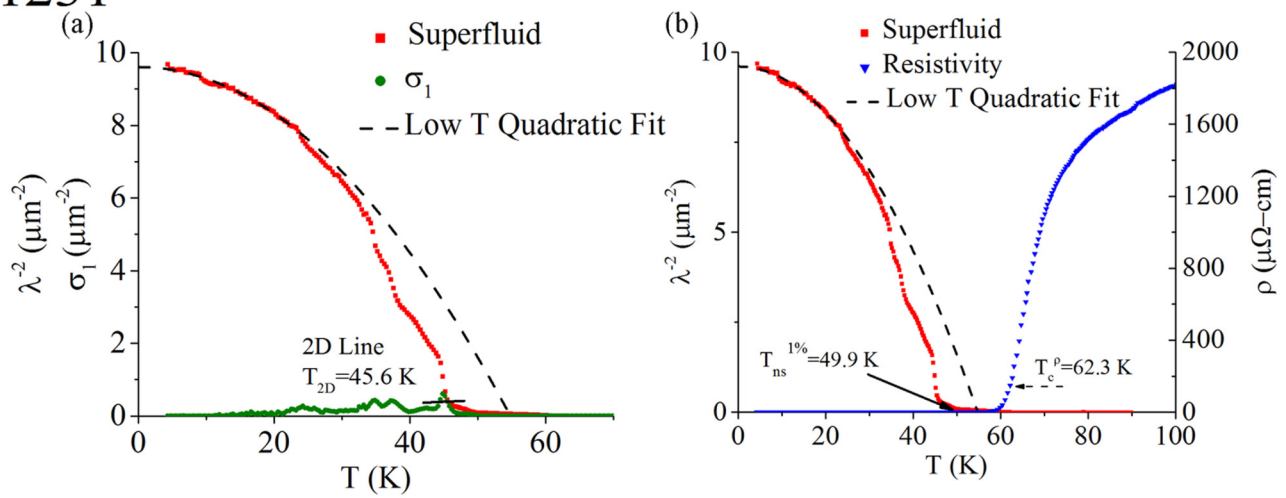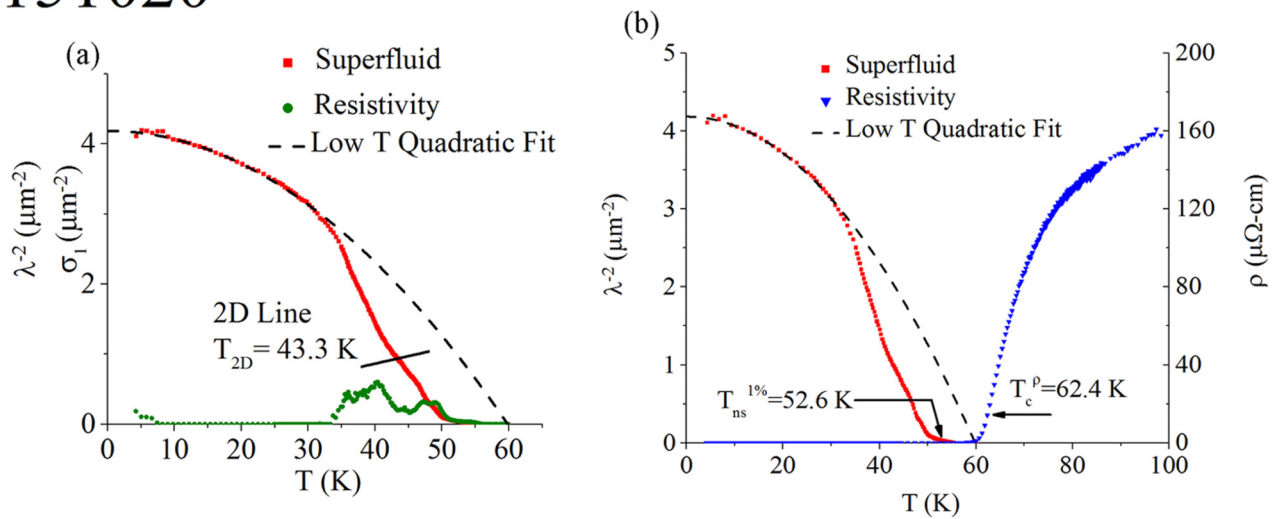FIG. 28. 10 uc film 1231.

151020

FIG. 29. 4 uc film 151020.
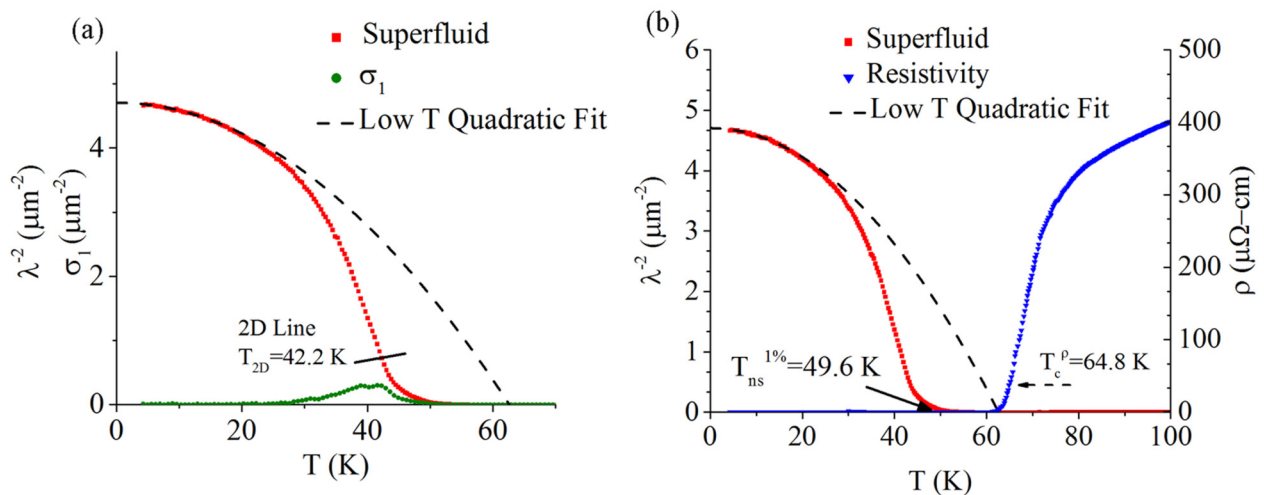
120807

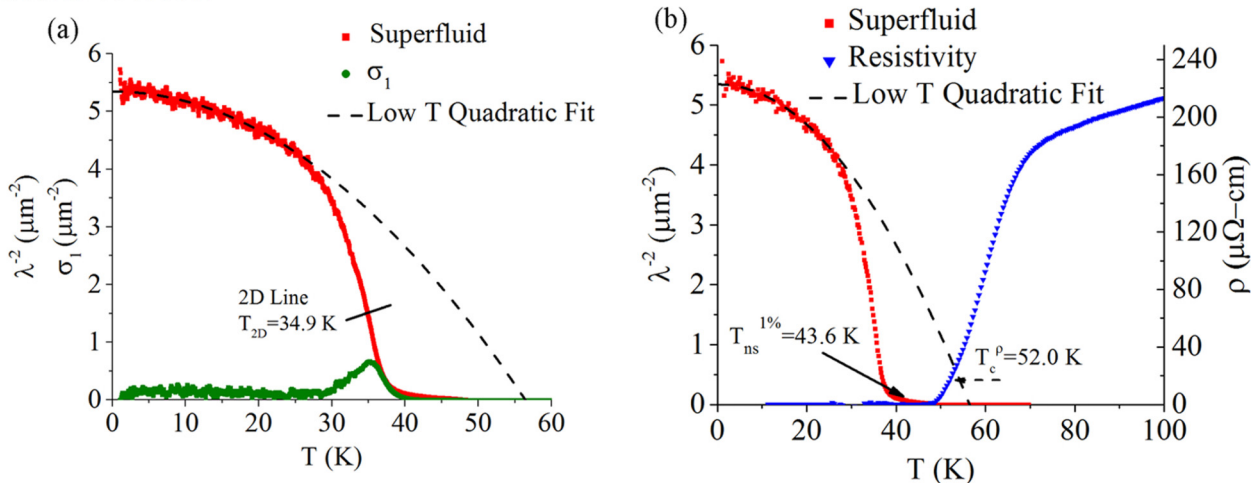FIG. 30. 5 uc film 120807.

Jon's Film

FIG. 31. 2 uc film "Jon's Film".
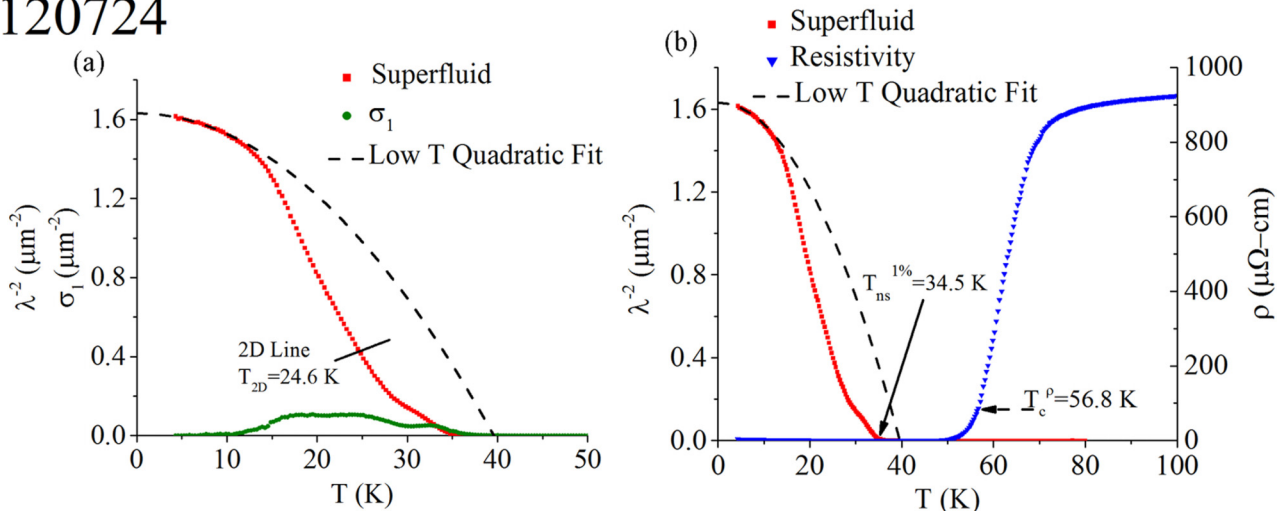
120724
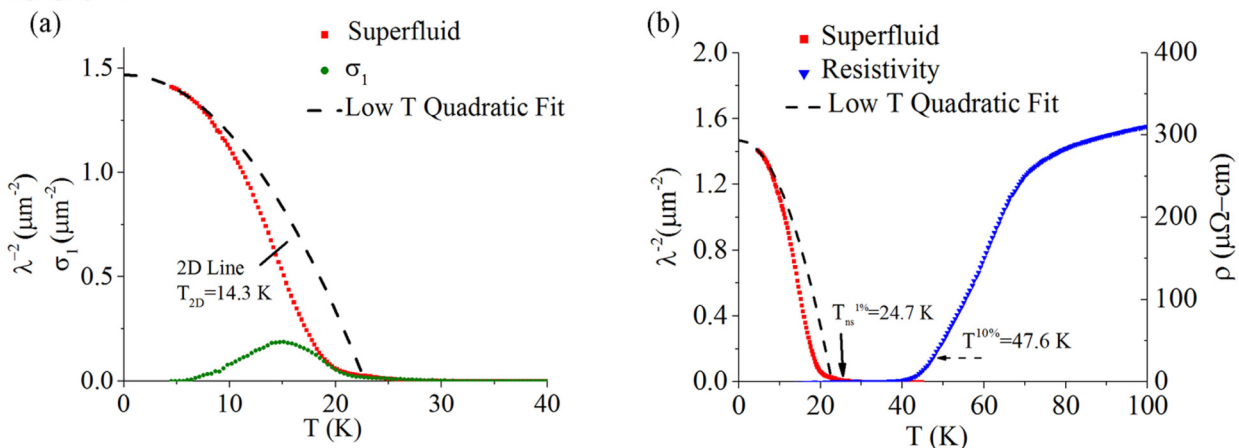

FIG. 32. 5 uc film 120724.

120802

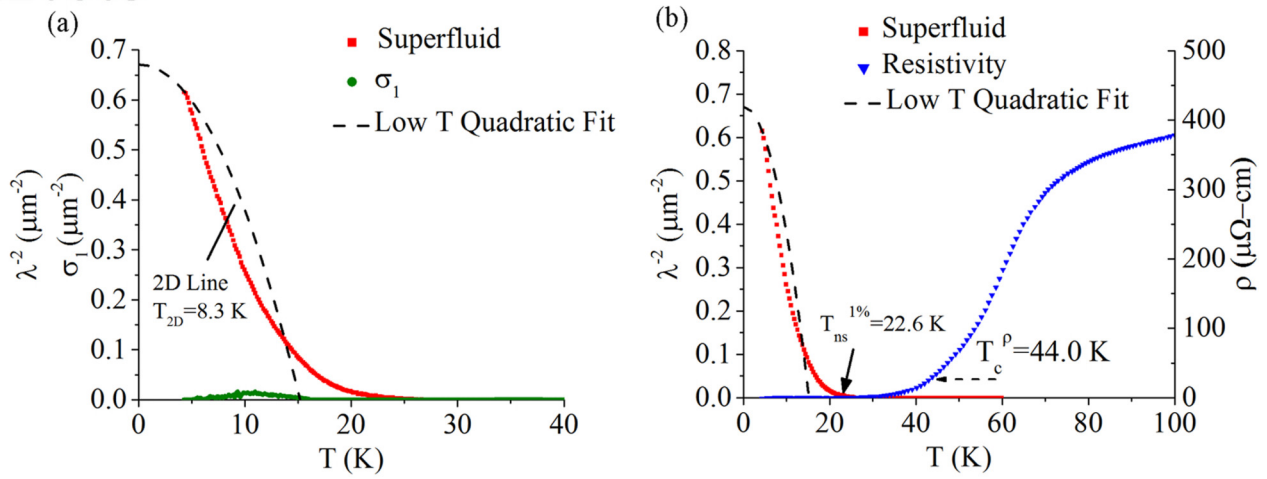FIG. 33. 2 uc film 120802.

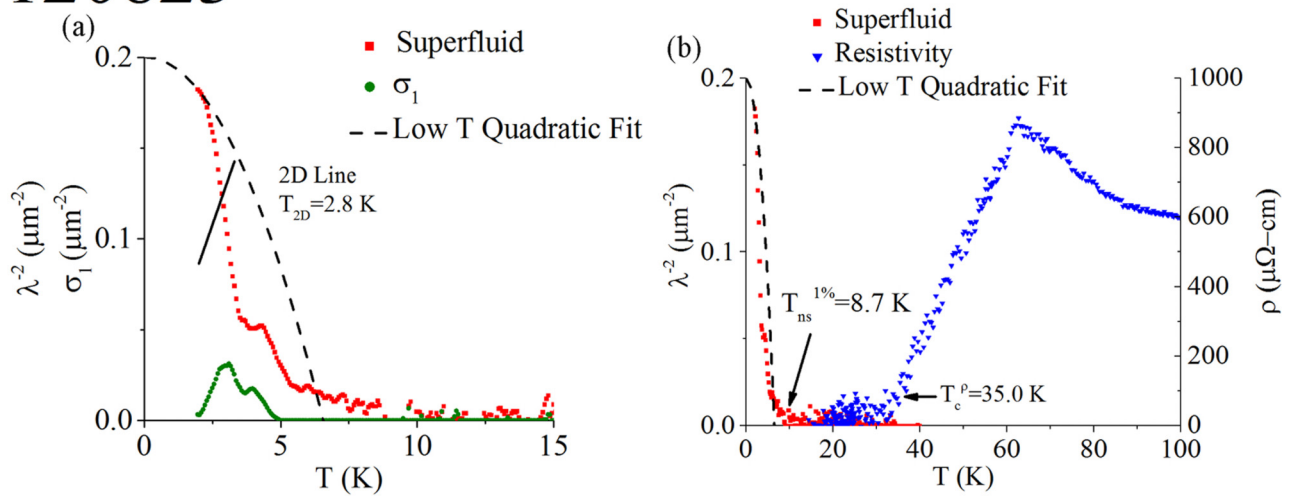## 120803

FIG. 34. 2 uc film 120803.
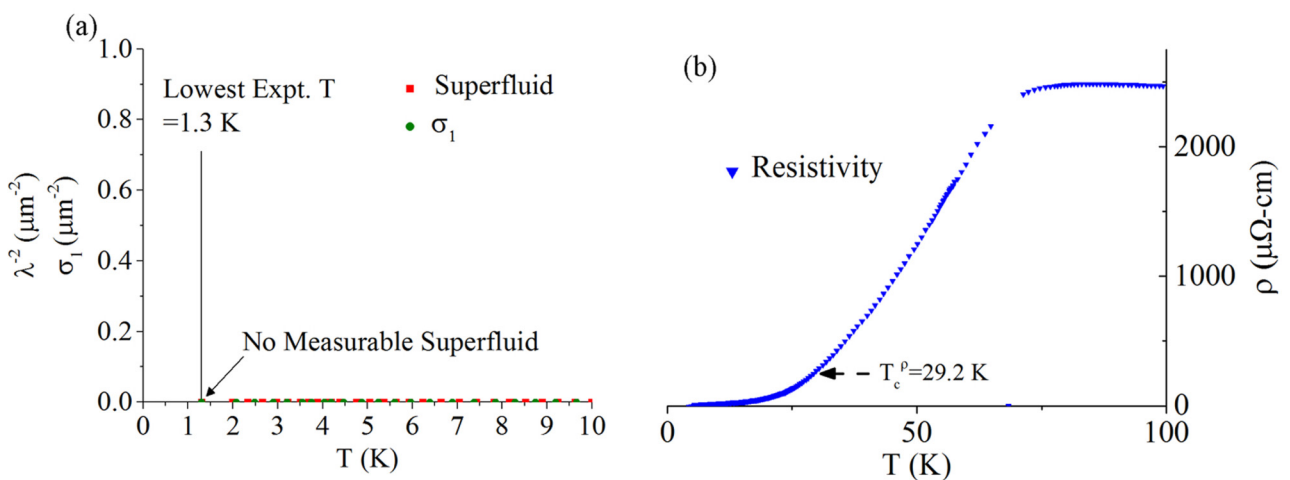
120823

FIG. 35. 2 uc film 120823.

120806

FIG. 36. 5 uc film 120806.

[1] I. Hetel, T. R. Lemberger, and M. Randeria, Nat. Phys. **3**, 700 (2007).

[2] Y. Zuev, M. S. Kim, and T. R. Lemberger, Phys. Rev. Lett. **95**, 137002 (2005).

[3] J. M. Kosterlitz and D. J. Thouless, J. Phys. C: Solid State Phys. **5**, 124 (1972).

[4] J. M. Kosterlitz and D. J. Thouless, J. Phys. C: Solid State Phys. **6**, 1181 (1973).

[5] V. L. Berezinskii, Sov. Phys. JETP **34**, 610 (1972).

[6] D. W. Abraham, C. J. Lobb, M. Tinkham, and T. M. Klapwijk, Phys. Rev. B **26**, 5268 (1982).

[7] B. I. Halperin and D. R. Nelson, J. Low Temp. Phys. **36**, 599 (1979).

[8] S. Caprara, M. Grilli, L. Benfatto, and C. Castellani, Phys. Rev. B **84**, 014514 (2011).

[9] M. Mondal, S. Kumar, M. Chand, A. Kamlapure, G. Saraswat, G. Seibold, L. Benfatto, and P. Raychaudhuri, Phys. Rev. Lett. **107**, 217003 (2011).

[10] J. Yong, T. R. Lemberger, L. Benfatto, K. Ilin, and M. Siegel, Phys. Rev. B **87**, 184505 (2013).

[11] L. Benfatto, C. Castellani, and T. Giamarchi, Phys. Rev. B **80**, 214506 (2009).

[12] P. G. Baity, X. Shi, Z. Shi, L. Benfatto, and D. Popović, Phys. Rev. B **93**, 024519 (2016).

[13] S. J. Turneaure, A. A. Pesetski, and T. R. Lemberger, J. Appl. Phys. **83**, 4334 (1998).

[14] Y. L. Zuev, J. A. Skinta, M.-S. Kim, T. R. Lemberger, E. Wertz, K. Wu, and Q. Li, Phys. C (Amsterdam) **468**, 276 (2008).

[15] G. Blatter, M. V. Feigel'man, V. B. Geshkenbein, A. I. Larkin, and V. M. Vinokur, Rev. Mod. Phys. **66**, 1125 (1994).

[16] J. Yong, M. J. Hinton, A. McCray, M. Randeria, M. Naamneh, A. Kanigel, and T. R. Lemberger, Phys. Rev. B **85**, 180507 (2012).

[17] Y. L. Zuev, Studies of thermal phase fluctuations in severely underdoped YBCO films, Ph.D. thesis, The Ohio State University, 2005.

[18] U. Kabasawa, Y. Tarutani, M. Okamoto, T. Fukazawa, A. Tsukamoto, M. Hiratani, and K. Takagi, Phys. Rev. Lett. **70**, 1700 (1993).

[19] Y. Suzuki, J. M. Triscone, C. B. Eom, M. R. Beasley, and T. H. Geballe, Phys. Rev. Lett. **73**, 328 (1994).

[20] B. Wuyts, V. V. Moshchalkov, and Y. Bruynseraede, Phys. Rev. B **53**, 9418 (1996).

[21] L. Benfatto, C. Castellani, and T. Giamarchi, Phys. Rev. B **77**, 100506 (2008).

[22] I. N. Hetel, Quantum critical behavior in the superfluid density of high-temperature superconducting thin films, Ph.D. thesis, The Ohio State University, 2008.

[23] C. Leemann, P. Fluckiger, V. Marsico, J. L. Gavilano, P. K. Srivastava, P. Lerch, and P. Martinoli, Phys. Rev. Lett. **64**, 3082 (1990).

[24] G. Seibold, L. Benfatto, C. Castellani, and J. Lorenzana, Phys. Rev. Lett. **108**, 207004 (2012).

[25] R. Ganguly, D. Chaudhuri, P. Raychaudhuri, and L. Benfatto, Phys. Rev. B **91**, 054514 (2015).

[26] Q. Li, M. Hucker, G. D. Gu, A. M. Tsvelik, and J. M. Tranquada, Phys. Rev. Lett. **99**, 067001 (2007).

[27] E. Fradkin, S. A. Kivelson, and J. M. Tranquada, Rev. Mod. Phys. **87**, 457 (2015).

[28] J. Weng, Q. Jie, Q. Li, M. Hucker, M. v. Zimmermann, S. J. Han, Z. Xu, D. K. Singh, R. M. Konik, L. Zhang, G. Gu, and J. M. Tranquada, Phys. Rev. B **85**, 134513 (2012).

[29] R. Beyers and T. M. Shaw, Solid State Phys. **42**, 135 (1989).

[30] M. J. Hinton, J. Yong, S. Steers, and T. R. Lemberger, J. Supercond. Nov. Magn. **26**, 2617 (2013).